AMADEUS—The acoustic neutrino detection test system of the ANTARES deep-sea neutrino telescope

J.A. Aguilar [a], I. Al Samarai [b], A. Albert [c], M. Anghinolfi [d], G. Anton [e], S. Anvar [f], M. Ardid [g], A.C. Assis Jesus [h], T. Astraatmadja [h,1], J.-J. Aubert [b], R. Auer [e], E. Barbarito [i], B. Baret [j], S. Basa [k], M. Bazzotti [l,m], V. Bertin [b], S. Biagi [l,m], C. Bigongiari [a], M. Bou-Cabo [b], M.C. Bouwhuis [h], A. Brown [b], J. Brunner [b,2], J. Busto [b], F. Camarena [g], A. Capone [n,o], C. Cârloganu [p], G. Carminati [l,m], J. Carr [b], B. Cassano [i], E. Castorina [q,r], V. Cavasinni [q,r], S. Cecchini [m,s], A. Ceres [i], Ph. Charvis [t], T. Chiarusi [m], N. Chon Sen [c], M. Circella [i], R. Coniglione [u], H. Costantini [d], N. Cottini [v], P. Coyle [b], C. Curtil [b], G. De Bonis [n,o], M.P. Decowski [h], I. Dekeyser [w], A. Deschamps [t], C. Distefano [u], C. Donzaud [j,x], D. Dornic [b,a], D. Drouhin [c], T. Eberl [e], U. Emanuele [a], J.-P. Ernenwein [b], S. Escoffier [b], F. Fehr [e], C. Fiorello [i], V. Flaminio [q,r], U. Fritsch [e], J.-L. Fuda [w], P. Gay [p], G. Giacomelli [l,m], J.P. Gómez-González [a], K. Graf [e], G. Guillard [y], G. Halladjian [b], G. Hallewell [b], H. van Haren [z], A.J. Heijboer [h], E. Heine [h], Y. Hello [t], J.J. Hernández-Rey [a], B. Herold [e], J. Hößl [e], M. de Jong [h,1], N. Kalantar-Nayestanaki [aa], O. Kalekin [e], A. Kappes [e], U. Katz [e], P. Keller [b], P. Kooijman [h,ab,ac], C. Kopper [e], A. Kouchner [j], W. Kretschmer [e], R. Lahmann [e,*], P. Lamare [f], G. Lambard [b], G. Larosa [g], H. Laschinsky [e], H. Le Provost [f], D. Lefèvre [w], G. Lelaizant [b], G. Lim [h,ac], D. Lo Presti [ad], H. Loehner [aa], S. Loucatos [v], F. Louis [f], F. Lucarelli [n,o], S. Mangano [a], M. Marcelin [k], A. Margiotta [l,m], J.A. Martinez-Mora [g], A. Mazure [k], M. Mongelli [i], T. Montaruli [i,ae], M. Morganti [q,r], L. Moscoso [v,j], H. Motz [e], C. Naumann [v,4], M. Neff [e], R. Ostasch [e], D. Palioselitis [h], G.E. Păvălaş [af], P. Payre [b], J. Petrovic [h], N. Picot-Clemente [b], C. Picq [v], V. Popa [af], T. Pradier [y], E. Presani [h], C. Racca [c], A. Radu [af], C. Reed [b,h], G. Riccobene [u], C. Richardt [e], M. Rujoiu [af], M. Ruppi [i,3], G.V. Russo [ad], F. Salesa [a], P. Sapienza [u], F. Schöck [e], J.-P. Schuller [v], R. Shanidze [e], F. Simeone [o], M. Spurio [l,m], J.J.M. Steijger [h], Th. Stolarczyk [v], M. Taiuti [ag,d], C. Tamburini [w], L. Tasca [k], S. Toscano [a], B. Vallage [v], V. Van Elewyck [j], G. Vannoni [v], M. Vecchi [n,b], P. Vernin [v], G. Wijnker [h], E. de Wolf [h,ac], H. Yepes [a], D. Zaborov [ah], J.D. Zornoza [a], J. Zúñiga [a]

[a] IFIC - Instituto de Física Corpuscular, Edificios Investigación de Paterna, CSIC - Universitat de València, Apdo. de Correos 22085, 46071 Valencia, Spain
[b] CPPM - Centre de Physique des Particules de Marseille, CNRS/IN2P3 et Université de la Méditerranée, 163 Avenue de Luminy, Case 902, 13288 Marseille Cedex 9, France
[c] GRPHE - Institut Universitaire de Technologie de Colmar, 34 rue du Grillenbreit BP 50568, 68008 Colmar, France
[d] INFN - Sezione di Genova, Via Dodecaneso 33, 16146 Genova, Italy
[e] Friedrich-Alexander-Universität Erlangen-Nürnberg, Erlangen Centre for Astroparticle Physics, Erwin-Rommel-Str. 1, 91058 Erlangen, Germany
[f] Direction des Sciences de la Matière - Institut de Recherche sur les lois fondamentales de l'Univers - Service d'Electronique des Détecteurs et d'Informatique, CEA Saclay, 91191 Gif-sur-Yvette Cedex, France
[g] Institut d'Investigació per a la Gestió Integrada de Zones Costaneres (IGIC) - Universitat Politècnica de València. C/ Paranimf 1., 46730 Gandia, Spain
[h] FOM Instituut voor Subatomaire Fysica Nikhef, Science Park 105, 1098 XG Amsterdam, The Netherlands
[i] INFN - Sezione di Bari, Via E. Orabona 4, 70126 Bari, Italy
[j] APC - Laboratoire AstroParticule et Cosmologie, UMR 7164 (CNRS, Université Paris 7 Diderot, CEA, Observatoire de Paris) 10, rue Alice Domon et Léonie Duquet, 75205 Paris Cedex 13, France
[k] LAM - Laboratoire d'Astrophysique de Marseille, Pôle de l'Étoile Site de Château-Gombert, rue Frédéric Joliot-Curie 38, 13388 Marseille Cedex 13, France
[l] Dipartimento di Fisica dell'Università, Viale Berti Pichat 6/2, 40127 Bologna, Italy
[m] INFN - Sezione di Bologna, Viale Berti Pichat 6/2, 40127 Bologna, Italy
[n] Dipartimento di Fisica dell'Università La Sapienza, P.le Aldo Moro 2, 00185 Roma, Italy
[o] INFN - Sezione di Roma, P.le Aldo Moro 2, 00185 Roma, Italy
[p] Clermont Université, Université Blaise Pascal, CNRS/IN2P3, Laboratoire de Physique Corpusculaire, BP 10448, 63000 Clermont-Ferrand, France
[q] Dipartimento di Fisica dell'Università, Largo B. Pontecorvo 3, 56127 Pisa, Italy
[r] INFN - Sezione di Pisa, Largo B. Pontecorvo 3, 56127 Pisa, Italy
[s] INAF-IASF, via P. Gobetti 101, 40129 Bologna, Italy
[t] Géoazur - Université de Nice Sophia-Antipolis, CNRS/INSU, IRD, Observatoire de la Côte d'Azur and Université Pierre et Marie Curie, BP 48, 06235 Villefranche-sur-mer, France
[u] INFN - Laboratori Nazionali del Sud (LNS), Via S. Sofia 62, 95123 Catania, Italy
[v] Direction des Sciences de la Matière - Institut de recherche sur les lois fondamentales de l'Univers - Service de Physique des Particules, CEA Saclay, 91191 Gif-sur-Yvette Cedex, France
[w] COM - Centre d'Océanologie de Marseille, CNRS/INSU et Université de la Méditerranée, 163 Avenue de Luminy, Case 901, 13288 Marseille Cedex 9, France
[x] Université Paris-Sud 11 - Département de Physique, 91403 Orsay Cedex, France

[y] IPHC - Institut Pluridisciplinaire Hubert Curien - Université de Strasbourg et CNRS/IN2P3 23 rue du Loess, BP 28, 67037 Strasbourg Cedex 2, France
[z] Royal Netherlands Institute for Sea Research (NIOZ), Landsdiep 4, 1797 SZ 't Horntje (Texel), The Netherlands
[aa] Kernfysisch Versneller Instituut (KVI), University of Groningen, Zernikelaan 25, 9747 AA Groningen, The Netherlands
[ab] Universiteit Utrecht, Faculteit Betawetenschappen, Princetonplein 5, 3584 CC Utrecht, The Netherlands
[ac] Universiteit van Amsterdam, Instituut voor Hoge-Energie Fysika, Science Park 105, 1098 XG Amsterdam, The Netherlands
[ad] Dipartimento di Fisica ed Astronomia dell'Università, Viale Andrea Doria 6, 95125 Catania, Italy
[ae] University of Wisconsin, Madison, WI 53715, USA
[af] Institute for Space Sciences, R-77125 Bucharest, Măgurele, Romania
[ag] Dipartimento di Fisica dell'Università, Via Dodecaneso 33, 16146 Genova, Italy
[ah] ITEP - Institute for Theoretical and Experimental Physics, B. Cheremushkinskaya 25, 117218 Moscow, Russia

ARTICLE INFO

ABSTRACT

The AMADEUS (ANTARES Modules for the Acoustic Detection Under the Sea) system which is described in this article aims at the investigation of techniques for acoustic detection of neutrinos in the deep sea. It is integrated into the ANTARES neutrino telescope in the Mediterranean Sea. Its acoustic sensors, installed at water depths between 2050 and 2300 m, employ piezo-electric elements for the broad-band recording of signals with frequencies ranging up to 125 kHz. The typical sensitivity of the sensors is around -145 dB re 1 V/μPa (including preamplifier). Completed in May 2008, AMADEUS consists of six "acoustic clusters", each comprising six acoustic sensors that are arranged at distances of roughly 1 m from each other. Two vertical mechanical structures (so-called lines) of the ANTARES detector host three acoustic clusters each. Spacings between the clusters range from 14.5 to 340 m. Each cluster contains custom-designed electronics boards to amplify and digitise the acoustic signals from the sensors. An on-shore computer cluster is used to process and filter the data stream and store the selected events. The daily volume of recorded data is about 10 GB. The system is operating continuously and automatically, requiring only little human intervention. AMADEUS allows for extensive studies of both transient signals and ambient noise in the deep sea, as well as signal correlations on several length scales and localisation of acoustic point sources. Thus the system is excellently suited to assess the background conditions for the measurement of the bipolar pulses expected to originate from neutrino interactions.

1. Introduction

Measuring acoustic pressure pulses in huge underwater acoustic arrays is a promising approach for the detection of cosmic neutrinos with energies exceeding 100 PeV. The pressure signals are produced by the particle cascades that evolve when neutrinos interact with nuclei in water. The resulting energy deposition in a cylindrical volume of a few centimetres in radius and several metres in length leads to a local heating of the medium which is instantaneous with respect to the hydrodynamic time scales. This temperature change induces an expansion or contraction of the medium depending on its volume expansion coefficient. According to the thermo-acoustic model [1,2], the accelerated motion of the heated volume—a micro-explosion—forms a pressure pulse of bipolar shape which propagates in the surrounding medium. Coherent superposition of the elementary sound waves, produced over the volume of the energy deposition, leads to a propagation within a flat disc-like volume (often referred to as *pancake*) in the direction perpendicular to the axis of the particle cascade. After propagating several hundreds of metres in sea water, the pulse has a characteristic frequency spectrum that is expected to peak around 10 kHz [3–5]. Given the strongly anisotropic propagation pattern of the sound waves, the details of the pressure pulse, namely its amplitude, asymmetry and frequency spectrum, depend on the distance and angular position of the observer with respect to the particle cascade

induced by the neutrino interaction [3]. Besides sea water, which is the medium under investigation in the case of the AMADEUS (ANTARES Modules for the Acoustic Detection Under the Sea) project, ice [6] and fresh water [7] are investigated as media for acoustic detection of neutrinos. Studies in sea water are also pursued by other groups using military arrays of hydrophones (i.e. underwater microphones) [8,9] or exploiting other existing deep sea infrastructures [10].

Two major advantages over an optical neutrino telescope motivate studying acoustic detection. First, the attenuation length in sea water is about 5 km (1 km) for 10 kHz (20 kHz) signals. This is one to two orders of magnitude larger than for visible light with a maximum attenuation length of about 60 m. The second advantage is the more compact sensor design and simpler readout electronics for acoustic measurements. Since on the other hand the speed of sound[5] is small compared to the speed of light, coincidence windows between two spatially separated sensors are correspondingly large. Furthermore, the signal amplitude is relatively small compared to the acoustic background in the sea, resulting in a high trigger rate at the level of individual sensors and making the implementation of efficient online data reduction techniques essential. To reduce the required processing time without sacrificing the advantages given by the large attenuation length, the concept of spatially separated clusters of acoustic sensors is used in AMADEUS. Online data filtering is then predominantly applied to the closely arranged sensors within a cluster.

The AMADEUS project was conceived to perform a feasibility study for a potential future large-scale acoustic neutrino detector. For this purpose, a dedicated array of acoustic sensors was

---

* Corresponding author. Tel.: +49 9131 8527147.
  E-mail address: robert.lahmann@physik.uni-erlangen.de (R. Lahmann).
[1] Also at University of Leiden, the Netherlands.
[2] On leave at DESY, Platanenallee 6, 15738 Zeuthen, Germany.
[3] Now at Altran Italia, Corso Sempione 66, 20100 Milano, Italy.
[4] Now at LPNHE - Laboratoire de Physique Nucléaire et des Hautes Énergies, UMR 7585, 4 place Jussieu - 75252 Paris Cedex 05, France.

[5] The speed of sound in sea water depends on temperature, salinity and pressure, i.e. depth. A good guideline value for the speed of sound at the location of AMADEUS is 1500 m/s.

integrated into the ANTARES neutrino telescope [11,12]. In the context of AMADEUS, the following aims are being pursued:

- Long-term background investigations (levels of ambient noise, spatial and temporal distributions of sources, rate of neutrino-like signals).
- Investigation of spatial correlations for transient signals and for persistent background on different length scales.
- Development and tests of data filter and reconstruction algorithms.
- Investigation of different types of acoustic sensors and sensing methods.
- Studies of hybrid (acoustic and optical) detection methods.

In particular the knowledge of the rate and correlation length of neutrino-like acoustic background events is a prerequisite for estimating the sensitivity of a future acoustic neutrino detector.

The focus of this paper is the AMADEUS system within the ANTARES detector. In Section 2, an overview of the system is given, with particular emphasis on its integration into the ANTARES detector. In Section 3, the system components are described and in Section 4 the system performance is discussed. The characteristic features of the AMADEUS system are mainly determined by the acoustic sensors and the custom-designed electronics board, which performs the off-shore processing of the analogue signals from the acoustic sensors. These two components are discussed in detail in Sections 3.1 and 3.4.

2. Overview of the AMADEUS system

2.1. The ANTARES detector and its sub-system AMADEUS

AMADEUS is integrated into the ANTARES neutrino telescope [11,12], which was designed to detect neutrinos by measuring the Cherenkov light emitted along the tracks of relativistic secondary muons generated in neutrino interactions. A sketch of the detector, with the AMADEUS modules highlighted, is shown in Fig. 1. The detector is located in the Mediterranean Sea at a water depth of about 2500 m, about 40 km south of the town of Toulon
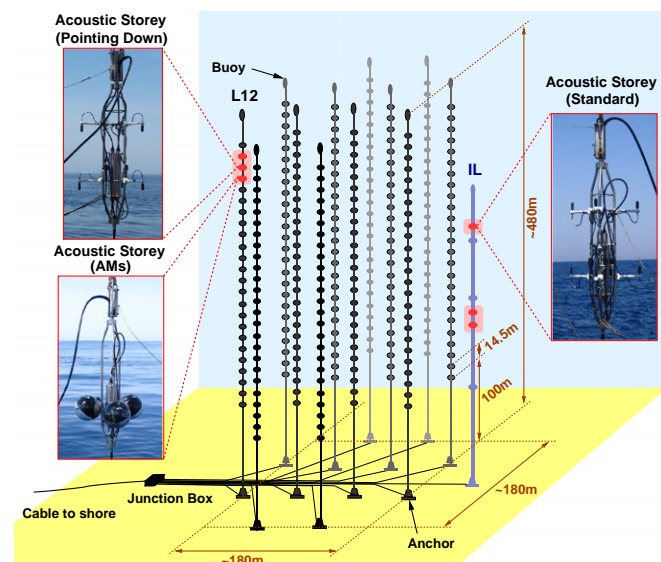

Fig. 1. A sketch of the ANTARES detector. The six acoustic storeys are highlighted and their three different setups are shown (see text for details). L12 and IL denote the 12th detection line and the Instrumentation Line, respectively.

on the French coast and was completed in May 2008. It comprises 12 vertical structures, the *detection lines*. Each detection line holds up to 25 *storeys* that are arranged at equal distances of 14.5 m along the line, starting at about 100 m above the sea bed and interlinked by electro-optical cables. A standard storey consists of a titanium support structure, holding three *Optical Modules* [13] (each one consisting of a photomultiplier tube (PMT) inside a water-tight pressure-resistant glass sphere) and one *Local Control Module* (*LCM*). The LCM consists of a cylindrical titanium container and the off-shore electronics within that container (see Section 3.3).

A 13th line, called *Instrumentation Line* (*IL*), is equipped with instruments for monitoring the environment. It holds six storeys. For two pairs of consecutive storeys in the IL, the vertical distance is increased to 80 m. Each line is fixed on the sea floor by an anchor equipped with electronics and held taut by an immersed buoy. An interlink cable connects each line to the *Junction Box* from where the main electro-optical cable provides the connection to the shore station.

The ANTARES lines are free to swing and twist in the undersea current. In order to determine the positions of the storey with a precision of about 20 cm—which is necessary to achieve the required pointing precision for neutrino astronomy—the detector is equipped with an acoustic positioning system [14]. The system employs an acoustic transceiver at the anchor of each line and four autonomous transponders positioned around the 13 lines. Along each detection line, five positioning hydrophones receive the signals emitted by the transceivers. By performing multiple time delay measurements and using these to triangulate the positions of the individual hydrophones, the line shapes can be reconstructed relative to the positions of the emitters. Currently, the sequence of positioning emissions is repeated every 2 min.

In AMADEUS, acoustic sensing is integrated in the form of *acoustic storeys* that are modified versions of standard ANTARES storeys, in which the Optical Modules are replaced by custom-designed acoustic sensors. Dedicated electronics is used for the digitisation and pre-processing of the analogue signals. The acoustic storeys are equivalent to the acoustic clusters introduced in Section 1.

The AMADEUS system comprises a total of six acoustic storeys: three on the IL, which started data taking in December 2007, and three on the 12th detection line (Line 12), which was connected to shore in May 2008. AMADEUS is now fully functional and routinely taking data with 34 sensors. Two out of 36 hydrophones became inoperational during their deployment. In both cases, the defect was due to pressurisation.

The acoustic storeys on the IL are located at 180, 195, and 305 m above the sea floor. On Line 12, which is anchored at a horizontal distance of about 240 m from the IL, the acoustic storeys are positioned at heights of 380, 395, and 410 m above the sea floor. With this setup, the maximum distance between two acoustic storeys is 340 m. AMADEUS hence covers three length scales: spacings of the order of 1 m between sensors within a storey (i.e. an acoustic cluster); intermediate distances of 14.5 m between adjacent acoustic storeys within a line; and large scales from about 100 m vertical distance on the IL up to 340 m between storeys on different lines. The sensors within a cluster allow for efficient triggering of transient signals and for direction reconstruction. The combination of the direction information from different acoustic storeys yields (after verifying the consistency of the signal arrival times at the respective storeys) the position of an acoustic source [15]. The AMADEUS system includes time synchronisation and a continuously operating data acquisition setup and is in principle scalable to a large-volume detector.
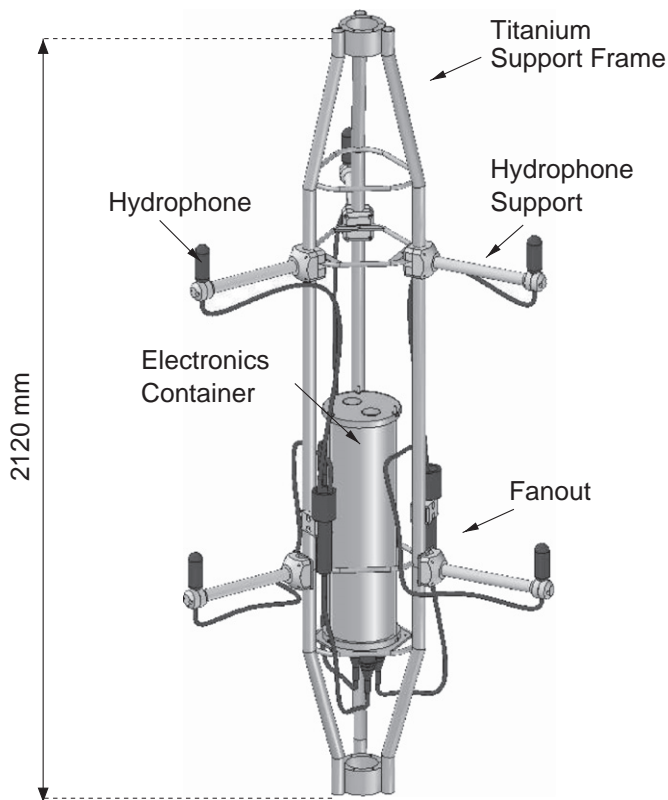
Fig. 2. Drawing of a standard acoustic storey, or acoustic cluster, with hydrophones.

2.2. Acoustic storeys

Two types of sensing devices are used in AMADEUS: hydrophones and *Acoustic Modules* (AMs). The sensing principle is in both cases based on the piezo-electric effect and is discussed in Section 3.1. For the hydrophones, the piezo-elements are coated in polyurethane, whereas for the AMs they are glued to the inside of standard glass spheres which are normally used for Optical Modules. Fig. 2 shows the design of a standard acoustic storey with hydrophones.

Fig. 3 shows the three different designs of acoustic storeys installed in AMADEUS. The acoustic storeys on the IL house hydrophones only, whereas the lowermost acoustic storey of Line 12 holds AMs. The hydrophones are mounted to point upwards, except for the central acoustic storey of Line 12, where they point downwards. The sensitivity of the hydrophones is largely reduced at their cable junctions and therefore shows a strong dependence on the polar angle. The different configurations allow for investigating the anisotropy of ambient noise, which is expected to originate mainly from the sea surface.

Three of the five storeys holding hydrophones are equipped with commercial models, dubbed "HTI hydrophones",[6] and the other two with hydrophones, described in detail in Section 3.1, developed and produced at the Erlangen Centre for Astroparticle Physics (ECAP).

2.3. Design principles

A fundamental design guideline for the AMADEUS system has been to use existing ANTARES hardware and software as much as

---

[6] Custom produced by High Tech Inc (HTI) in Gulfport, MS (USA).

possible. This eases the operation of the system within the environment of the ANTARES neutrino telescope; at the same time, the design efforts were kept to a minimum and new quality assurance and control measures had to be introduced only for the additional components. These were subjected to intensive testing procedures, in particular in view of the hostile environment due to the high water pressure of up to 240 bar and the salinity of the water.

In order to integrate the AMADEUS system into the ANTARES neutrino telescope, design and development efforts in the following basic areas were necessary:

- The development of acoustic sensing devices that replace the Optical Modules of standard ANTARES storeys and of the cables to route the signals into the electronics container.
- The development of an off-shore acoustic digitisation and pre-processing board.
- The setup of an on-shore server cluster for the online processing of the acoustic data and the development of the online software.
- The development of offline reconstruction and simulation software.

Six acoustic sensors per storey were implemented. This number was the maximum compatible with the design of the LCM and the bandwidth of data transmission to shore. Furthermore, the acoustic storeys were designed such that their size did not exceed the size of the standard ANTARES storeys in radial dimension, hence assuring compatibility with the deployment procedure of the ANTARES lines.

2.4. The AMADEUS-0 test apparatus

In March 2005, a full-scale mechanical prototype line for the ANTARES detector was deployed and subsequently recovered [16]. This line, dubbed *Line 0*, contained no photomultipliers and no readout electronics. Instead, an autonomous data logging system and shore-based optical time-domain reflectometry were used to record the status of the setup.

Line 0 provided a well-suited environment to study the properties of the acoustic sensors in situ at a time when the readout electronics for AMADEUS was still in the planning phase and the piezo-preamplifier setup in the design phase. For this purpose, an autonomous system within a standard LCM container, the *AMADEUS-0* device, was integrated into Line 0. It recorded acoustic signals at the ANTARES site using five piezo-sensors with custom-designed preamplifiers with an overall sensitivity of about $-120\,dB\,re\,1\,V/\mu\,Pa$ in the range from 5 to 50 kHz, glued to the inside of the LCM container. A battery-powered readout and data logging system was devised and implemented using commercially available components. The system was further equipped with a timing mechanism to record data over two pre-defined periods: The first one lasted for about 10 h and included the deployment of the line. During this period, a total of 2:45 h of data were recorded over several intervals. In the second period, with the line installed on the sea floor, 1:45 h of data were taken over a period of 3:30 h until the battery power was exhausted.

The analysis of the data [17] provided valuable information for the design of the AMADEUS system. In particular, the level of the recorded noise allowed for tuning the sensitivity and frequency response of the preamplifiers and amplifiers. A filtered amplitude distribution is shown in Fig. 4, where signals saturating the readout electronics have been removed. The Gaussian fit shown in the figure is a measure of the combined ambient noise of the deep sea and inherent noise of the system, while the excess of data is
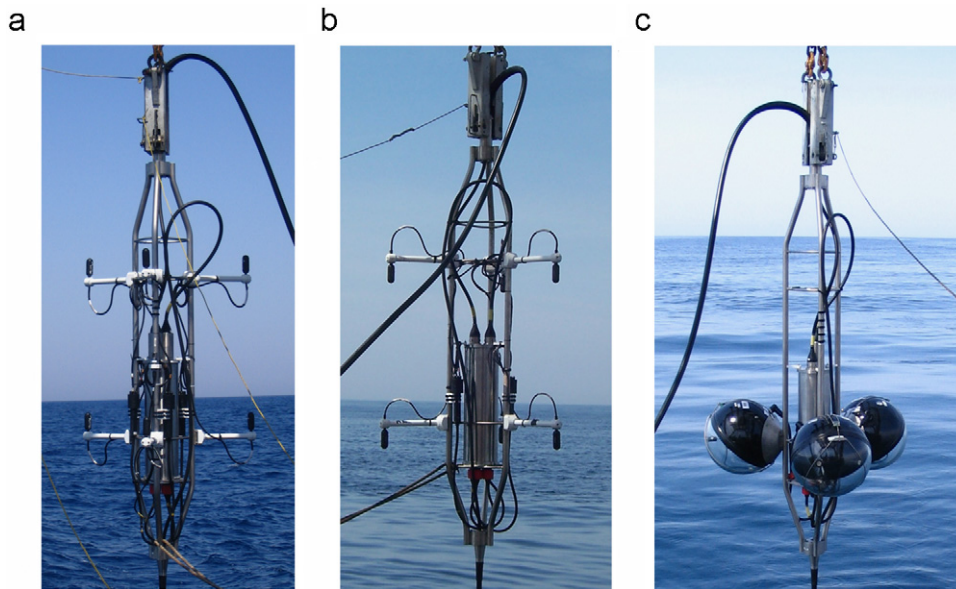
Fig. 3. Photographs of three different storeys of the AMADEUS system during their deployment: (a) standard storey, equipped with hydrophones pointing up; (b) the central acoustic storey on Line 12 with the hydrophones pointing down; and (c) the lowermost acoustic storey on Line 12 equipped with Acoustic Modules.
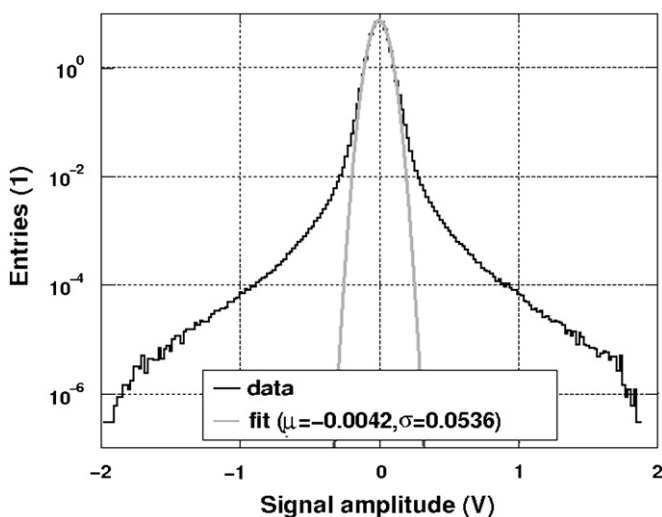
Fig. 4. Normalised distribution of signal amplitudes for all data recorded with the AMADEUS-0 device. High amplitude ($>$ 2 V) signals, saturating the readout electronics, have been removed. A Gaussian fit to the data yields mean μ and standard deviation σ.

due to transient signals. This shows that the sensitivity of the system is well matched to record background noise while at the same time allowing for a wide dynamic range of transient signals. A comparable overall sensitivity was hence chosen for the AMADEUS setup. The design of the commercial readout electronics proved to be not suitable in terms of long-term stability and the response to signals that saturated the readout electronics. This experience was returned to the design of the AMADEUS readout electronics, which will be described in Section 3.4.

3. System components

3.1. The acoustic sensors

The fundamental components of both the hydrophones and the AMs, collectively referred to as acoustic sensors, are piezo-electrical ceramic elements, converting pressure waves into voltage signals [18], and preamplifiers. In this subsection, the hydrophones, the AM sensors, and the calibration of their sensitivity will be discussed.

3.1.1. Hydrophones

A schematic drawing of an ECAP hydrophone is shown in Fig. 5. For these hydrophones,[7] two-stage preamplifiers were used: adapted to the capacitive nature of the piezo-elements and the low induced voltages, the first preamplifier stage is charge integrating while the second one is amplifying the output voltage of the first stage. The shape of the ceramics is that of a hollow cylinder.

Due to hardware constraints of the electronics container, the only voltage available for the operation of the preamplifiers was 6.0 V. In order to minimise electronic noise, the preamplifiers were designed for that voltage rather than employing DC/DC converters to obtain the 12.0 V supply typically used.

The piezo-elements and preamplifiers of the hydrophones are coated in polyurethane. Plastic endcaps prevent the material from pouring into the hollow part of the piezo-cylinder during the moulding procedure. The ECAP as well as the HTI hydrophones have a diameter of 38 mm and a length (from the cable junction to the opposite end) of 102 mm.

The equivalent inherent noise level in the frequency range from 1 to 50 kHz is about 13 mPa for the ECAP hydrophones and about 5.4 mPa for the HTI hydrophones. This compares to 6.2 mPa of the lowest expected ambient noise level in the same frequency band for a completely calm sea [19], referred to as *sea state 0* [20].

At the ANTARES site, the hydrophones are subject to an external pressure of 210 to 240 bar, depending on the depth at which they are installed. Prior to deployment, each hydrophone was pressure-tested in accordance with the standard ANTARES procedure, i.e. the pressure was ramped up to 310 bar at 12 bar/min, held there for two hours and then ramped down again at 12 bar/min.

---

[7] For the commercial hydrophones, details were not disclosed by the manufacturer, but the main design is similar to the one described here.
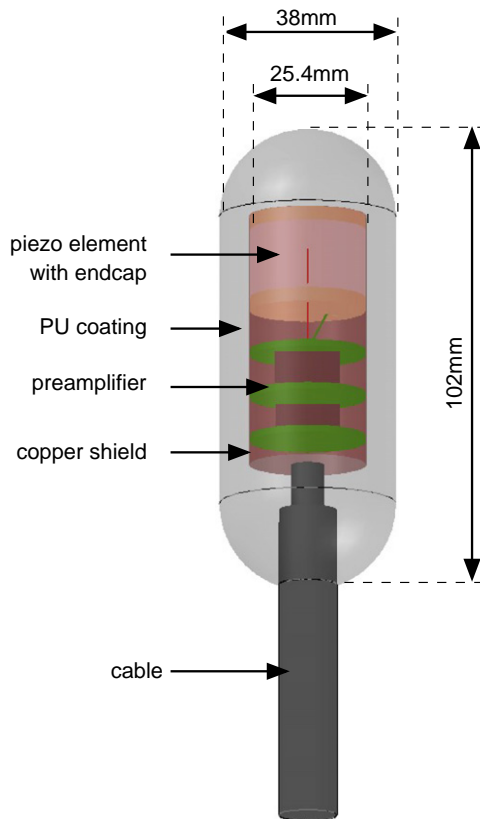
Fig. 5. Schematic drawing of an ECAP hydrophone. Piezo-element and preamplifier (consisting of three circular circuit boards, interconnected by pin connectors) are moulded into polyurethane (PU).

3.1.2. Acoustic modules

For the AMs, the same preamplifiers are used as for the ECAP hydrophones. The piezo-elements have the same outer diameter but are solid cylinders in case of the AMs. Two sensors are glued to the inside of each sphere. This design was motivated by the idea to operate the piezo-elements at low pressure and also to investigate an option for acoustic sensing that can be integrated together with a PMT in the same glass sphere. In order to assure a good acoustic coupling, the space between the curved sphere and the flat end of the piezo-sensor of the AMs was filled with epoxy. A photograph of an Acoustic Module and a schematic drawing of the sensors glued to the inside of the glass sphere are shown in Figs. 6(a) and (b), respectively.

In order to obtain a 2π azimuthal coverage, the six sensors are distributed over the three AMs of the storey within the horizontal plane defined by the three centres of the spheres as shown in Fig. 6(c). The spheres have outer diameters of 432 mm.

3.1.3. Calibration

All sensors are tuned to have a low noise level and to be sensitive over the frequency range from 1 to 50 kHz with a typical sensitivity around -145 dB re 1 V/μ Pa (including preamplifier). The sensitivities of all sensors as a function of frequency, polar angle and azimuthal angle were measured before deployment in a water tank, using a calibrated emitter [21]. The analysis was restricted to frequencies above 10 kHz. Towards lower frequencies, measurements become increasingly less significant. This is due to the quadratic frequency dependence of the emitter's transmit voltage response and to the increasingly adverse effect of reflections for increasing wavelengths. In accordance with the

expected behaviour of the piezo-elements, the sensitivity is assumed to be constant below 10 kHz.

The sensitivity of one of the commercial hydrophones is shown in Fig. 7 as a function of frequency for different polar angles. For frequencies below 50 kHz, the sensitivity decreases once the polar angle approaches 180°, which defines the direction at which the cable is attached to the hydrophone. The beginning of this trend can be seen for the polar angle of 150°.

The sensitivity as a function of the azimuthal angle for a given frequency is essentially flat at the 3 dB level for all hydrophones. The sensitivity as a function of polar angle and frequency shows deviations of less than 2 dB between different HTI hydrophones in the frequency range from 10 to 50 kHz. The deviations for the hydrophones produced at ECAP are at a level of 3 to 4 dB. The sensitivity of an ECAP hydrophone is shown in Fig. 8. Compared to the HTI hydrophones, the sensitivity in the frequency range from 10 to 50 kHz is higher but less uniform, both as a function of frequency and as a function of polar angle.

As a consequence of their design, the solid angle over which the sensors of the AMs are sensitive is smaller compared to the hydrophones. Furthermore, reflections and resonances within the glass sphere affect the signal shape and frequency dependence, making laboratory measurements more difficult to interpret. The calibration was performed by varying the position of the emitter along a half circle, such that each emitter position has the same distance to the piezo-element. Angles were then given by the position of the emitter along the half circle with respect to the longitudinal axis of the piezo-sensor, which defined the angle of 0°. Results are shown in Fig. 9. The higher sensitivity compared to the ECAP hydrophones is due to the different piezo-element that is used and the acoustic coupling between water, the glass sphere and the piezo-sensor.

All sensitivity measurements were done at normal pressure. A verification with an in situ calibration has not yet been carried out at the time of the writing of this paper.

For the calibration that was describe above, Gaussian signals were emitted which in the frequency domain cover the range of the calibration. In addition, the response of the sensors to bipolar pulses was recorded. This is shown in Fig. 10. The agreement between the different sensor types is quite good. The asymmetry of the input pulse, i.e. the ratio of the pulse heights at the positive and negative peaks, can be seen to be diminished in the response of the sensors. This is due to the excitation of oscillations of the piezo-elements.

3.2. Cables and connectors

Each electronics container is equipped with three 12-pin SubConn connector sockets.[8] In order to connect two hydrophones to each of the three sockets, special *fanout cables* were produced (see Fig. 2). To the electronics container end of the cable, the same mating connector plugs are used as for the Optical Modules. At the other end of the cable, a bulkhead connector AWQ-4/24 of the ALL-WET split series by Seacon[9] was moulded, which fans out into six wedge-shaped sectors. Each sector has a 4-pin connector socket, serving the four leads for individual power supply and differential signal readout of the hydrophones. Each of the mating 4-pin connectors is moulded to a neoprene cable with the hydrophone at its other end. The remaining four sectors of the bulkhead connector are sealed with blind plugs.

The standard cables used in the ANTARES detector between the electronics container and the Optical Modules are also used to

---

[8] MacArtney Underwater Technology group, http://www.subconn.com/.
[9] Seacon (Europe) LTD, Great Yarmouth, Norfolk, UK, http://www.seaconeurope.com/.
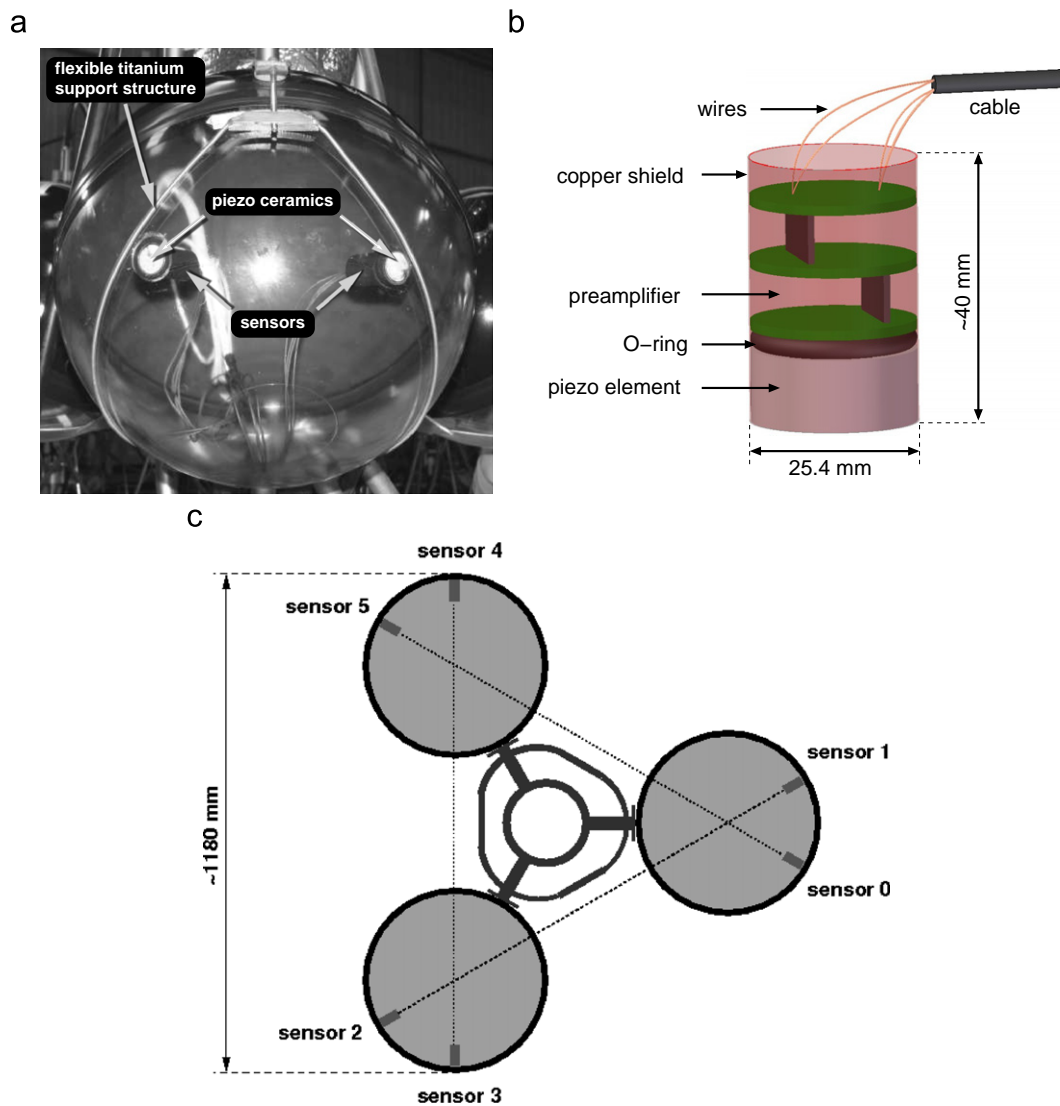
Fig. 6. (a) Photograph of an Acoustic Module (AM) before deployment; (b) schematic drawing of an AM sensor; and (c) horizontal cross-section of an acoustic storey holding Acoustic Modules in the plane of the sensors. The dotted lines are collinear with the longitudinal axes of the sensors and indicate the arrangement of the sensor within the storey. The lines intersect at angles of 60° at the centres of the glass spheres.

connect the AMs. The LCMs integrated into storeys with AMs and with hydrophones are interchangeable. All connections and cables within AMADEUS are functioning as expected.

3.3. Off-shore electronics

In the ANTARES data acquisition (DAQ) scheme [22], the digitisation is done within the off-shore electronics container (see Section 2). Each LCM contains a backplane that is equipped with sockets for the electronics cards and provides them with power and data lines. A standard LCM for processing the data from PMTs contains the following electronics boards:

- Three *ARS motherboards*, each comprising two Analogue Ring Sampler (ARS) ASICs, for conditioning and digitisation of the analogue signals from the PMTs [23].
- A *DAQ board*, which reads out the ARS motherboards and handles the communication to shore via TCP/IP.
- A *Clock board* that provides the timing signals to correlate measurements performed in different storeys (see Section 3.6).
- A *Compass board* to measure the tilt and the heading of the storey.

The transmission of data to shore is done through a *Master LCM (MLCM)* which—in addition to the components of an LCM described above—contains an ethernet switch and additional boards for handling incoming and outgoing fibre-based optical data transmission. Up to five storeys form a *sector*, in which the individual LCMs transmit the data to the MLCM.

For the digitisation of the acoustic signals and for feeding them into the ANTARES data stream, the *AcouADC board* was designed. These boards are pin-compatible with the ARS motherboards and replace them in the acoustic storeys. Fig. 11 shows the fully equipped LCM of an acoustic storey.

3.4. The AcouADC board

Each AcouADC board serves two acoustic sensors and has the following major tasks:

- Pre-processing of the analogue signals (impedance matching, application of an anti-alias filter, selectable gain adjustment).
- Digitisation of the analogue signals and preparation of the digitised data stream for transmission to the DAQ board.
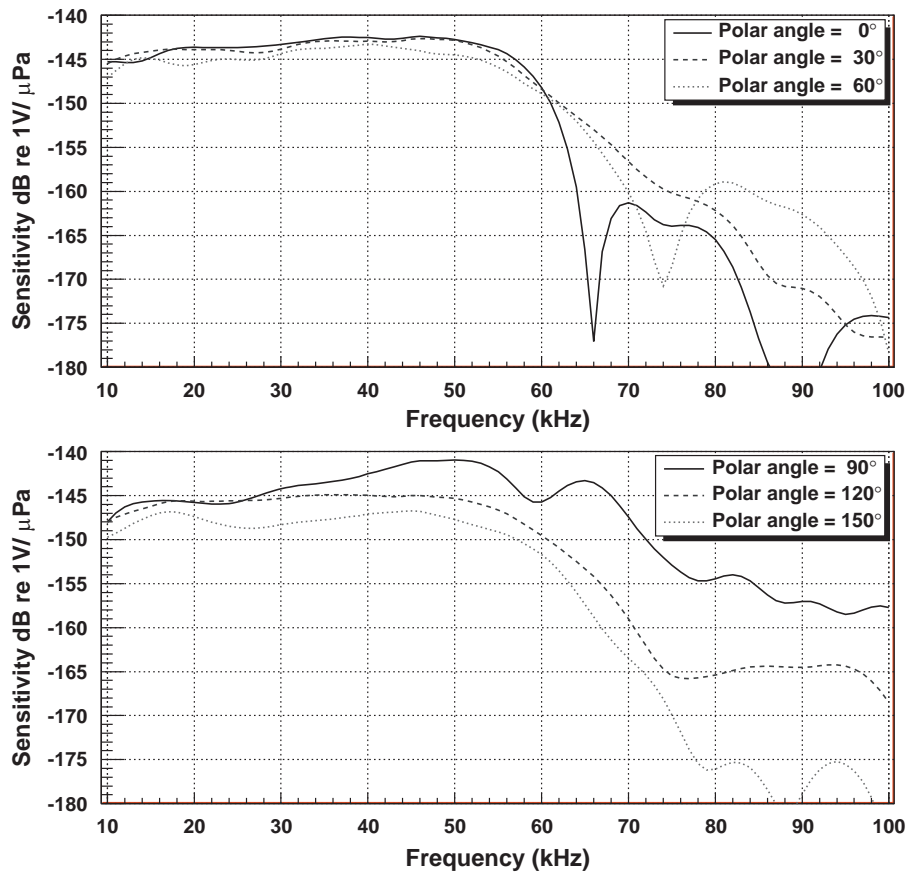
Fig. 7. Typical sensitivity of an HTI hydrophone as a function of frequency for different polar angles, averaged over the azimuthal angle. Systematic uncertainties below 50 kHz are 2–3 dB.

- Provision of stable low-noise voltage (6.0 V) for power supply of the acoustic sensors.
- Provision of an interface to the on-shore slow control software (see Section 3.5).

A photograph and a block diagram of an AcouADC board are shown in Figs. 12 and 13, respectively. The board consists of an analogue and a digital signal processing part. Each board processes the differential voltage signals from two acoustic sensors, referred to as "Sig 0" and "Sig 1" in the diagram. The two signals are processed independently and in parallel for the complete (analogue and digital) data processing chain.

A main design criterion for the board was a low inherent noise level, so that even for sea state 0 no significant contribution to the recorded signal originates from the electronics of the board. To protect the analogue parts from potential electromagnetic interference, they are shielded by metal covers. Tests of the electromagnetic compatibility (EMC) of the board have shown that this design is not significantly affected by electromagnetic noise even for conditions that are far more unfavourable than those present in situ [19].

The two 6.0 V power supply lines on each AcouADC board (connectors labelled "Pow 0" and "Pow 1" in Fig. 13) are protected by resettable fuses against short circuits that could be produced by the sensors due to water ingress. In addition, each voltage line can be individually switched on or off.

3.4.1. Analogue signal processing

The analogue signal is amplified in two stages. The first stage applies a coarse gain with nominal amplification factors of 1, 10 or 100. It is implemented as a differential amplifier with single-ended output, referenced to 2.5 V. The gain factor 1 is used for recording dedicated runs with large signal amplitudes, e.g. from the emitters of the ANTARES acoustic positioning system (see Section 2.1), whereas the factor of 100 was only foreseen for the case that the sensitivity of the hydrophones would degrade after deployment.

The second amplification stage, the fine gain, is intended to adjust the gains of different types of hydrophones. It is a non-inverting amplification with single ended output and a reference voltage of 2.5 V. Gain factors of 1.00, 1.78, 3.16, and 5.62 (corresponding to 0, 5, 10, and 15 dB, respectively) are selectable by switching between four appropriate resistors in the feedback loop of the operational amplifier. Combining the two stages, the gain factor can be set to one of 12 values between 1 and 562. The standard setting is an overall gain factor of 10, yielding the approximate sensitivity of -125 dB re 1 V/μ Pa.

After amplification, the signal is coupled into a linear-phase 10th-order anti-alias filter[10] with a root-raised cosine amplitude response and a 3 dB point at a frequency of 128 kHz. In low-power mode, the filter output range is about 3.9 V. The output is referenced to 2.0 V and fed into a 16-bit analogue-to-digital converter (ADC) that will be described below. Accordingly, the ADC reference voltage is set to 2.0 V, implying that the digital output of zero corresponds to this analogue value. The input range of the ADC is 0.0–4.0 V.

The three analogue stages (coarse and fine amplification and anti-alias filtering) and the ADC are decoupled by appropriate capacitors. Furthermore, several RCL elements within the

---

[10] Filter LTC1569-7 from Linear Technology, http://www.linear.com/.
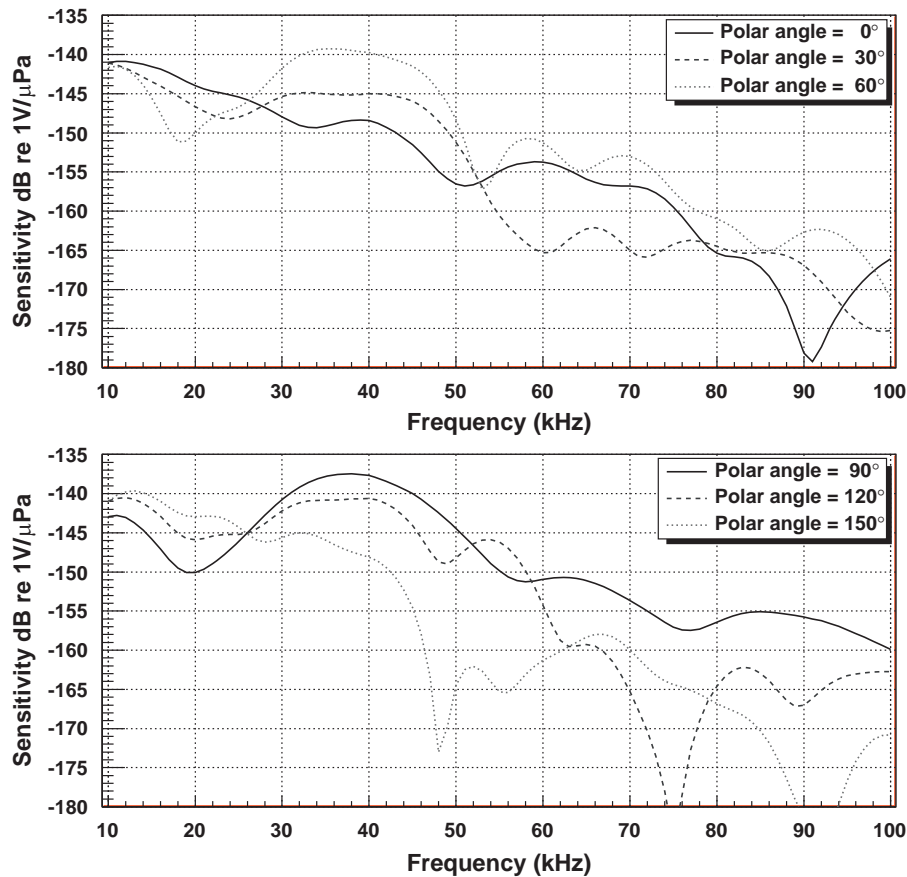
Fig. 8. Typical sensitivity of an ECAP hydrophone as a function of frequency for different polar angles, averaged over the azimuthal angle. Systematic uncertainties below 50 kHz are 2–3 dB.

analogue signal chain form an additional band-pass filter. Its low-frequency 3 dB point is at about 3 kHz and cuts into the trailing edge of the low-frequency noise of the deep-sea acoustic background [24], protecting the system from saturation. The high-frequency 3 dB point is above 1 MHz and was introduced to comply with the input requirements of active components of the circuitry.

3.4.2. Digital signal processing

The digital part of the AcouADC board digitises the acoustic signals and processes the digitised data. It is flexible due to the use of a micro controller (μC)[11] and a field programmable gate array (FPGA)[12] as data processor. All communication with the shore is done via the DAQ board; the μC handles the slow control (see Section 3.5) and the FPGA the data transfer. The μC is accessed from the on-shore control software and is used to adjust settings of the analogue part and the data processing. It can also be used to update the firmware of the FPGA. This firmware is stored in a flash memory and loaded after a reset of the FPGA. In situ, this reset is asserted from the μC. If a firmware update is performed, the μC first loads the code from the shore into the random access memory (RAM). Once the integrity of the code has been confirmed by means of a checksum, the code is transmitted into the flash memory. In order to avoid the potential risk that a software error renders the μC inaccessible, its boot memory can only be changed in the laboratory. For testing and programming

in the laboratory, JTAG[13] is used to access the FPGA, the μC, and the flash memory.

For each of the two input channels, the digitisation is done at 500 kS ps (kilosamples per second) by one 16-bit successive approximation ADC[14] with output range from $-32{,}768$ to $+32{,}767$ counts. The two ADCs are read out in parallel by the FPGA and further formatted for transmission to the DAQ board.

ADCs commonly show relatively high deviations from a linear behaviour near the zero value of their digital output. The size of this effect depends on the circuitry into which the ADC is embedded. For the prototypes of the AcouADC boards, this effect proved to be fairly pronounced. For this reason, the reference voltage of the anti-alias filter output can be switched from its standard value of 2.0–1.0 V, thereby moving the centre of the acoustic noise distribution away from the digital value of zero. This leads to an asymmetry of the recordable range for positive and negative amplitudes of acoustic signals, effectively reducing the dynamic range by a factor of 2 if one requires both positive and negative amplitudes to be fully recorded. For standard data taking, this is not desirable whereas the non-linearities of the ADCs proved to be unproblematic. Therefore, the reference voltage of the anti-alias filter output is set to 1.0 V only for special measurements.

In standard mode, the sampling rate is reduced to 250 kS ps in the FPGA, corresponding to a downsampling by a factor of 2 (DS2). Currently implemented options are DS1 (i.e. no downsampling),

---

[11] STR710 from STMicroelectronics, http://www.st.com/.
[12] Spartan-3 XC3S200 from XilinX, http://www.xilinx.com/.

[13] The IEEE standard 1149.1 "Test Access Port and Boundary-Scan Architecture" is commonly referred to as JTAG, the acronym for Joint Test Action Group. It defines an interface to individual components on a circuit board.
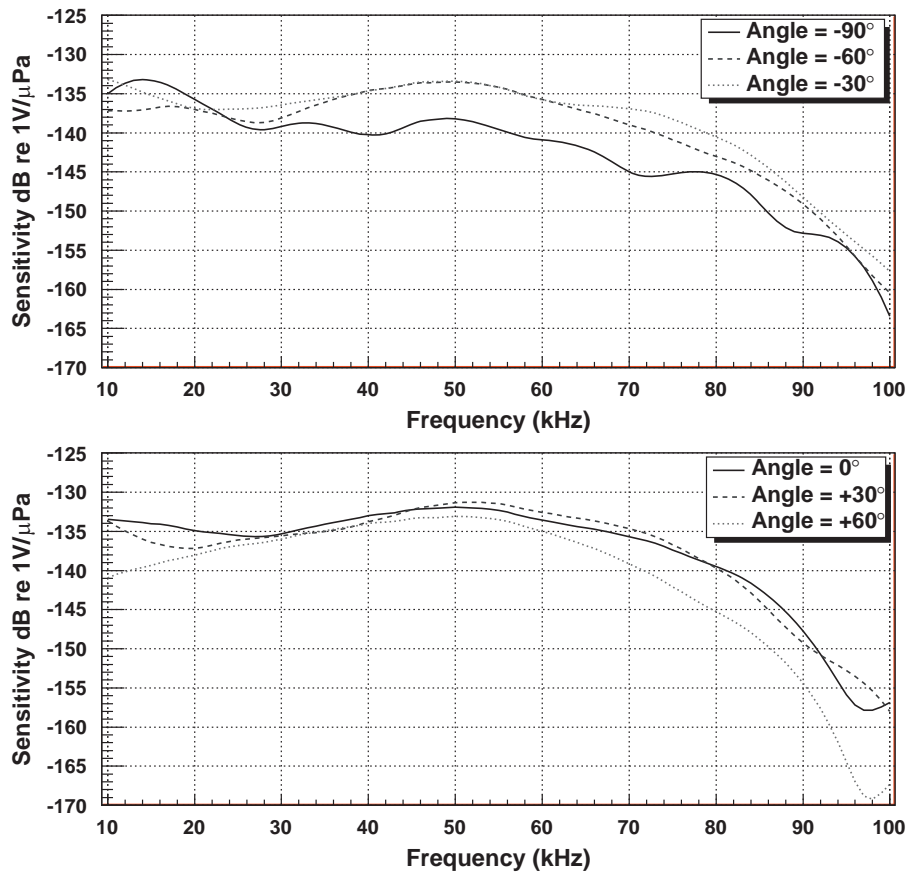[14] ADS8323 from Analogue Devices, http://www.analog.com/.

Fig. 9. Sensitivity of an AM sensor as a function of frequency for different angles with respect to the longitudinal axis of the sensor. Systematic uncertainties below 50 kHz are 2–3 dB.
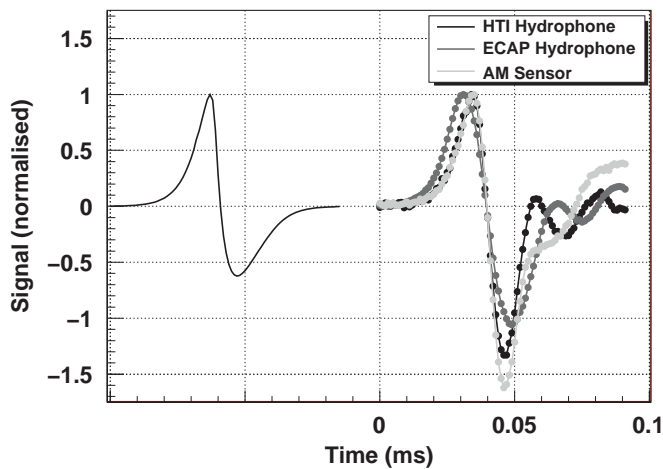

Fig. 10. Comparison of the response of different acoustic sensor types to a bipolar pulse. The emitted signal is shown on the left. The response of the hydrophones was measured for a polar angle of 90°, the response of the AM sensor for an angle of 0°. The first peak of each pulse (including the emitted one) was normalised to 1 and the time axis of each received signal was adjusted such that the times of the zero crossings coincide. The time offset between emitted and received pulses in the depiction is arbitrary.

DS2, and DS4, which can be selected from the shore. For each downsampling factor an adapted digital anti-alias filter, compliant with the Nyquist–Shannon sampling theorem, is implemented in the FPGA as a finite impulse response (FIR) filter with a length of 128 data points. For DS2, the frequency spectrum between the 3 dB points at 2.8 and 108.8 kHz passes the filter.

3.4.3. System characteristics

The complex response function of the AcouADC board (i.e. amplitude and phase) was measured in the laboratory prior to deployment for each board and a parametrisation of the function was derived [19]. Fig. 14 shows the frequency response of the AcouADC board. The measurement was done by feeding Gaussian white noise into the system and analysing the digital output recorded by the board. Without downsampling (DS1), the rolloff at high frequencies is governed by the analogue anti-alias filter. For DS2 and DS4, the digital FIR filters are responsible for the behaviour at high frequencies. At low frequencies, the effect of the band-pass filter described above can be seen. Fig. 14 furthermore demonstrates that within each passband, the filter response is essentially flat. The comparison of the recorded data with the parametrisation shows excellent agreement.

The parametrisation of the response function allows to calculate the response of the system to any input pulse and vice versa the reconstruction of the original shape of any recorded pulse. Fig. 15 shows a comparison of the measured and calculated response of the analogue signal processing part of the AcouADC board to a generic bipolar input pulse as it would be expected from a neutrino-induced cascade (see Section 1). The digital FIR filter introduces an additional time offset of 128 μs of the digitised data for DS2 and DS4.

The ADCs of the AcouADC board were investigated in detail [19]. For each individual ADC, the transfer curve from input voltage to ADC counts was measured and distortions from the ideal linear behaviour quantified in terms of the differential non-linearity (DNL) and integral non-linearity (INL). The distribution of the DNL values for all bins of all calibrated signal channels shows negligible deviations from the ideal situation (i.e. a peak at
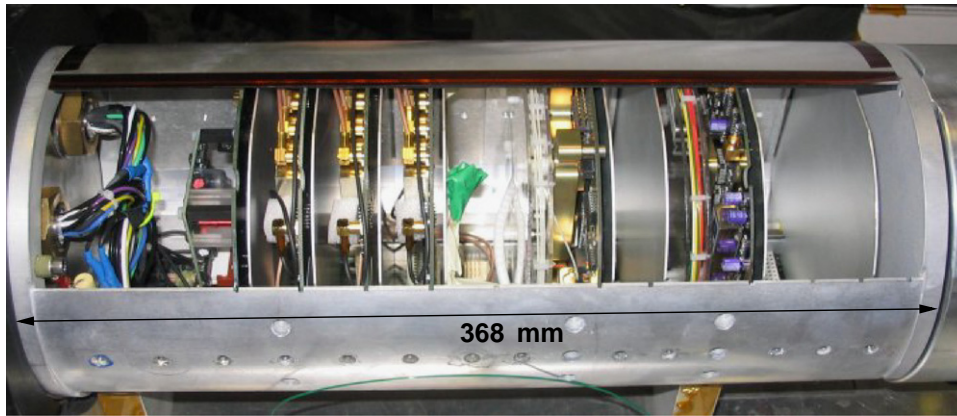
Fig. 11. An LCM during assembly, equipped with AcouADC boards before insertion into the titanium container. The sockets for external connection (not visible in this picture) are attached to the lid of the container on the left-hand side of the photograph. From left to right, the following boards are installed: a Compass board; three AcouADC boards; a DAQ board; and a Clock board.
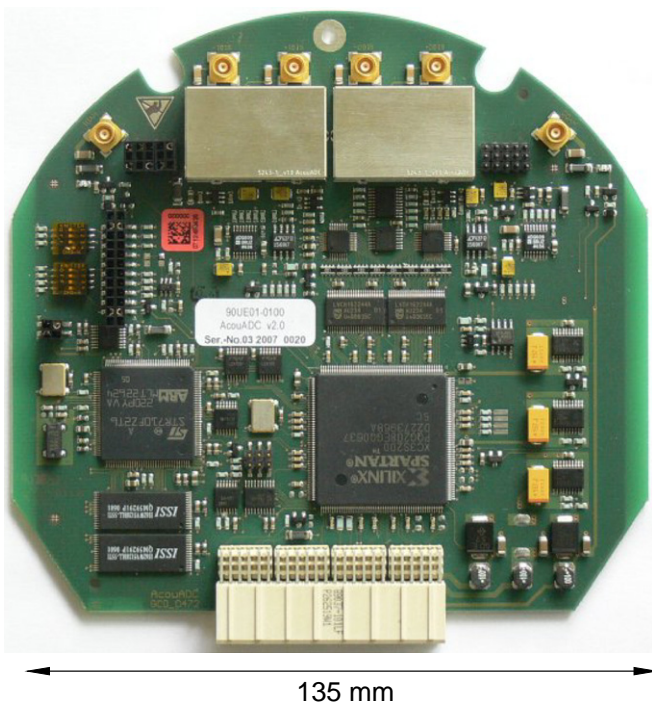
Fig. 12. Photograph of an AcouADC board. The four connectors for the two differential input signals are located at the top, the analogue signal processing electronics is covered by metal shields.

zero) with a mean of -0.02 ADC counts and a standard deviation of 0.06 ADC counts, corresponding to $3.4\,\mu V$. The values of the INL of the ADCs stay within ± 50 ADC counts for all signal channels over the full input range, corresponding to ± 3.1 mV.

The spurious-free dynamic range (SFDR) of an ADC is a measure of its dynamic range. Using a sinusoidal input signal, the average SFDR of the ADCs of all boards in AMADEUS was measured to be 59.9 ± 1.1 dB, meaning that harmonics of the sine wave distorting the output signal are suppressed by three orders of magnitude in the amplitude. Hence, a clear determination of the frequency is possible even for saturated signals, for which the harmonic components are enhanced.

The 12 gain factors for each channel were calibrated and the correction factor for gain 1 was measured to be 1.05 ± 0.01. The gain factors of the other 11 settings were measured with respect to this value and were found to deviate from the nominal factors by about 10% at maximum.

The inherent noise of the electronics (output for open signal input) and the cross-talk between the two signal channels of an AcouADC board were measured to be negligible in comparison with the inherent noise of the acoustic sensors.

3.5. Slow control system

The ANTARES slow control (SC) system has two main tasks. It provides the off-shore components with initialisation and configuration parameters and it regularly monitors whether the operational parameters are within their specified ranges. In addition, the readout of some instruments for environmental monitoring [25], performed at intervals of a few minutes, is polled and sent through the SC interface.

For the AMADEUS system, the following parameters can be set from shore via the SC system for each acoustic channel individually: one of the 12 values for the gain; downsampling factors of 1, 2, or 4 (or no data transmission from the AcouADC board); power supply for the acoustic sensor on or off; reference voltage of the analogue signal fed into the ADC 2.0 or 1.0 V.

To monitor the environment within each LCM container, a humidity sensor and temperature sensors on several boards are installed. One temperature sensor is placed on each AcouADC board. Values read out by the SC system are stored in an Oracle® database that is centrally used by ANTARES.

3.6. Data acquisition and clock system

AMADEUS uses the same DAQ system and follows the same "all data to shore" strategy [22] as the ANTARES neutrino telescope, i.e. all digitised data are transmitted to shore via optical fibres using the TCP/IP protocol. The data stream from the sender DAQ board is tagged with the IP address of the receiving on-shore server. In the control room, the acoustic data are routed to a dedicated computer cluster by using the transmitted IP address. The ANTARES clock system operates separately from the DAQ system, using a different set of optical fibres to synchronise data from different storeys. The system provides a highly stable 20 MHz synchronisation signal, corresponding to a resolution of 50 ns,[15] which is generated by a

---

[15] The much higher precision that is required for the synchronisation of the optical signals from the PMTs is provided by a 256-fold subdivision of the 20 MHz signal in the ARS motherboards.
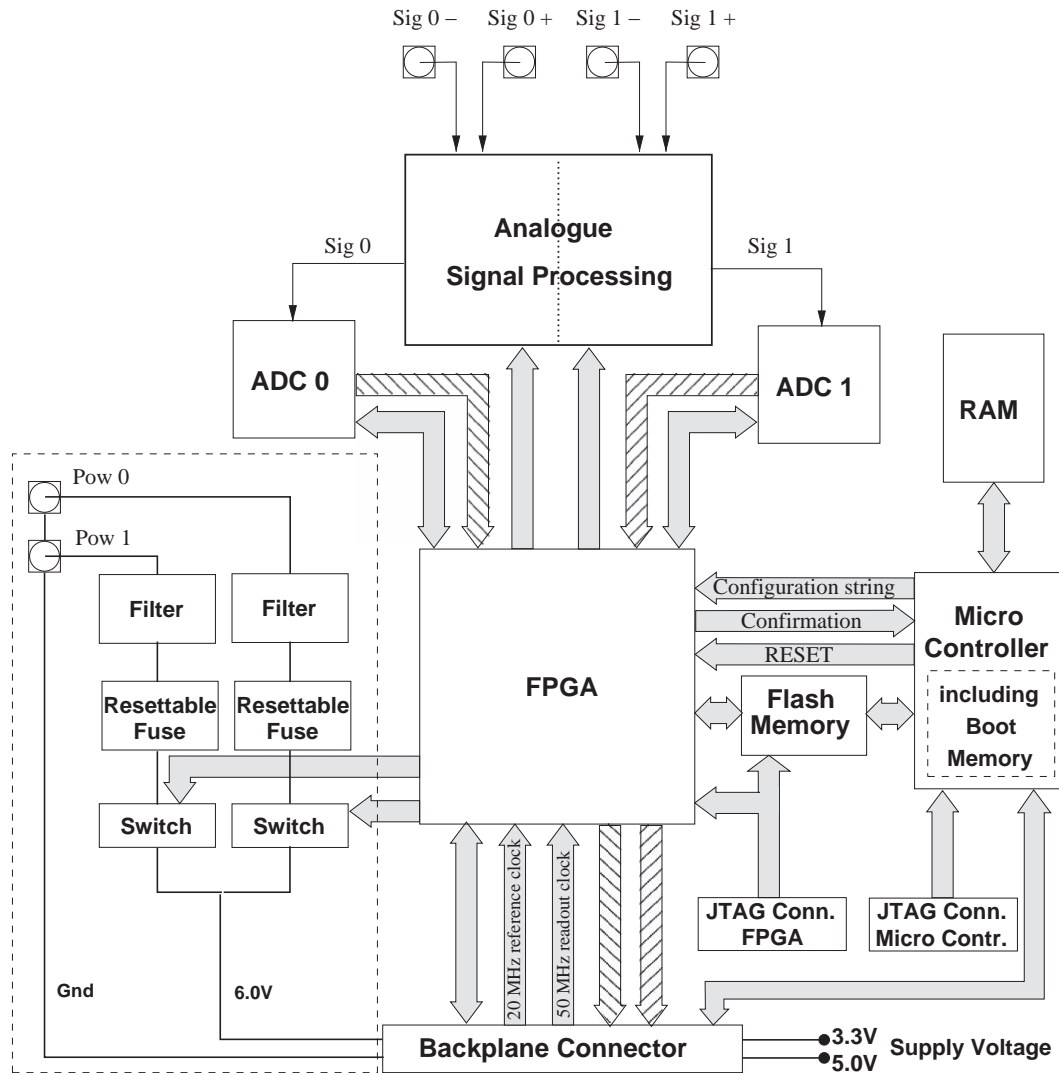
Fig. 13. Block diagram of the AcouADC board. The flow of the analogue sensor signals entering from the connectors (squares with inserted circles) at the top of the figure is indicated by thin arrows. Hatched arrows denote the flow of the digitised data further downstream. General communication connections are shown as shaded arrows. The components relevant for the power supply of the hydrophones are shown in the left part. Voltage supply lines are shown as thick lines, the dashed box indicates the circuitry for the power supply of the acoustic sensors.

custom-designed system at the ANTARES control room. The synchronisation of this internal clock with the UTC[16] of the GPS system is established with a precision of 100 ns.

The synchronisation signal is broadcast to the off-shore clock boards and from there transmitted further to the FPGA of the AcouADC board. Based on this signal, the data packages sent from the AcouADC board to shore via the DAQ board receive a timestamp which allows for correlating the data from different storeys. The 50 ns resolution of the timestamp by far exceeds the requirements given by the standard sampling time of 4 μs corresponding to DS2. Differences in the signal transit times between the shore station and the individual storeys are also smaller than 4 μs and do not need to be corrected for.

3.7. On-shore data processing and system operation

The AMADEUS system is operated with its own instance of the standard ANTARES control software called *RunControl* [22]. This is a programme with a graphical user interface to control and

operate the experiment. It is Java™–based and reads the configuration of the individual hard- and software components from the ANTARES database, allowing for an easy adaption of individual run parameters for the AMADEUS system. Via the clock system the absolute time of the run start is logged in the database with the aforementioned precision of 100 ns. The end of a run is reached if either the data volume or the duration exceed predefined limits (in which case a new run is started automatically) or the run is stopped by the operator. The data of one AMADEUS run are stored in a single file in *ROOT* format [26]. The typical duration of a run ranges from 2 to 5 h.

For the computing requirements of AMADEUS, a dedicated on-shore computer cluster was installed. It currently consists of four server-class computers, of which two are used for data triggering[17] (equipped with $2 \times$ dual core 3 GHz Intel Xeon 5160 and $2 \times$ quad core 3 GHz Intel Xeon 5450 processors, respectively). Hence, a total of 12 cores are available to process the data. One of the remaining two computers is used to write the data to an

---

[16] Coordinated Universal Time.

[17] While this functionality might be more commonly referred to as filtering, it is ANTARES convention to refer to the "on-shore trigger".
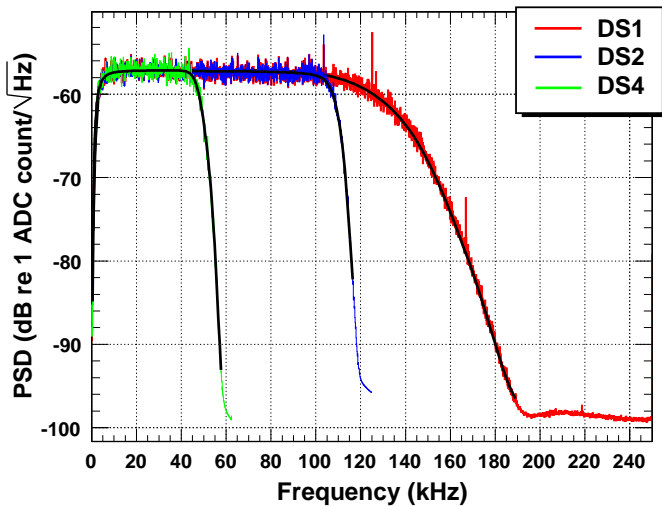
Fig. 14. The AcouADC board filter response, characterised by a power spectral density (PSD) as a function of frequency, measured for the three different downsampling factors. For each of the three measurements, the parametrisation is shown as a black line.
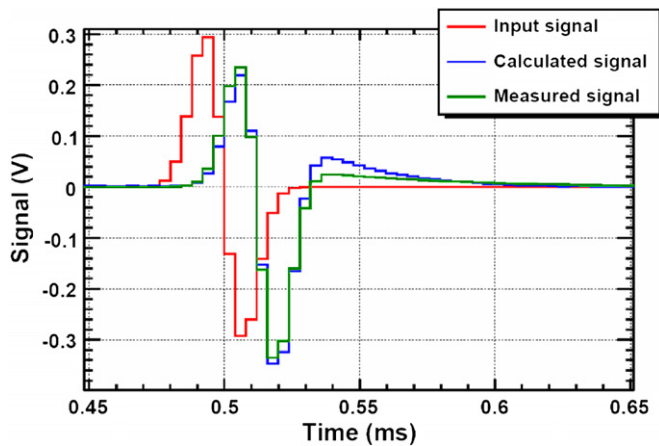

Fig. 15. The response of the analogue part of an AcouADC board to a bipolar input pulse. Shown are the measured output signal and the output signal calculated from the parametrised response function. The measured output signal was obtained with an oscilloscope at the input of the ADC. The measurement was done for a nominal gain factor of 1.

internal 550 GB disc array (RAID), while the other is used to operate the RunControl software and other miscellaneous processes and to provide remote access to the system via the Internet.

The AMADEUS trigger searches the data by an adjustable software filter; the events thus selected are stored to disc. This way the raw data rate of about 1.5 TB/day is reduced to about 10 GB/day for storage. Currently, three trigger schemes are in operation [27]: A minimum bias trigger which records data continuously for about 10 s every 60 min, a threshold trigger which is activated when the signal exceeds a predefined amplitude, and a pulse shape recognition trigger. For the latter, a cross-correlation of the signal with a predefined bipolar signal, as expected for a neutrino-induced cascade, is performed. The trigger condition is met if the output of the cross-correlation operation exceeds a predefined threshold. With respect to a matched filter, this implementation reduces the run time complexity while yielding a comparable trigger performance.

As discussed in Section 1, for pressure pulses induced by neutrino interactions the amplitude, asymmetry and frequency

spectrum depend on the position of the observer with respect to the particle cascade. The predefined bipolar signal used for the pulse shape recognition trigger corresponds to the pulse shape expected at a distance of roughly 300 m from the shower centre in the direction perpendicular to the shower axis, i.e. where the maximum signal within the flat volume of sound propagation is expected. The cross-correlation with pulses whose shape differs from the implemented one changes the peak in the cross-correlation output: it is broadened and diminished as compared to the filter response on the predefined signal. This effectively increases the trigger threshold in terms of pressure amplitude for such pulses. As will be described below, the final trigger decision requires coincidences within an acoustic storey, which allows the trigger threshold for the cross-correlation output of each individual acoustic sensor to be set to a low value. Given that the main purpose of the AMADEUS system is the investigation of background noise, this implementation is very efficient in recording a wide range of bipolar and multipolar events. Dedicated searches for neutrino signals—which are difficult due to the geometry of the acoustic storeys within the AMADEUS system—are done offline, taking into account the variations of the pulse shapes with distance and direction.

Both the threshold and the pulse shape recognition trigger are applied to the individual sensors and are self-adjusting to the ambient noise, implying that all trigger thresholds are defined in terms of a signal-to-noise ratio. The trigger thresholds are software parameters and therefore can be set at will. The noise level is calculated from and applied to the data of the *frame* that is currently being analysed. A frame denotes the structure in which data are buffered off-shore by the DAQ board before being sent to shore and contains data sampled during an interval of about 105 ms [22]. If one of these two trigger conditions is met, an additional trigger condition is imposed, which requires coincidences of a predefined number of acoustic sensors on each storey. The coincidence window is fixed to the length of a frame. Currently, the coincidence trigger requires that the threshold or pulse shape recognition trigger conditions have been met for at least four out of six sensors of a storey.

In the ANTARES DAQ system, the frames start at fixed intervals with respect to the run start. Trigger conditions are imposed on temporally corresponding frames from all storeys simultaneously, whereupon the frames are discarded and data not selected by the trigger are lost. Processing subsequent frames at the same time is not possible. Given the distances of typically 1 m between sensors within one storey, time delays between signals from a given source are always less than 1 ms. Therefore, the number of sources for which the signals extend over two frames, and hence the coincidence trigger may not be activated, is small. The disadvantage of a large trigger window, the increased probability for random coincidences, leads only to a small increase of the recorded data volume. The coincidence trigger can be optionally extended to require coincidences between different storeys on the same line. With distances between storeys ranging from about 10 to 100 m (corresponding to delays of the order of 10–100 ms) signals originating from above or below are suppressed. This trigger is currently not enabled.

The data of all sensors that have fired a coincidence trigger are stored within a common time window that covers all triggered signals. Its minimum length is 1.536 ms for 4 μs sampling time (corresponding to 384 data samples) and its maximum length corresponds to the length of a frame.

The triggers of the AMADEUS system and the main ANTARES optical neutrino telescope are working completely independently. Hence, the search for correlated signals relies on offline analyses.

Both the off-shore and on-shore part of the AMADEUS system are scalable, rendering it very flexible. The enlargement of the

system from three to six acoustic storeys with the commissioning of Line 12 (see Section 2.1) was easily implemented by increasing the on-shore computing power and updating the control software. In principle, the system could be upgraded to much bigger numbers of acoustic storeys. To reduce the data volume transmitted to shore, it would also be possible to move parts of the trigger algorithms into the FPGA of the AcouADC board.

AMADEUS is controlled remotely via the Internet. Data are centrally stored and are remotely available.

4. System performance

4.1. General

AMADEUS is continuously operating and taking data with only a few operator interventions per week. The up-time of each sensor is typically better than 80%. Its ability to continuously send unfiltered data, sampled at high frequency, to shore for further analysis renders the AMADEUS system a multipurpose apparatus for neutrino feasibility studies, acoustic positioning and marine research.

The concept of acoustic clusters (i.e. the acoustic storeys) is very beneficial for fast online processing. By requiring coincident signals from at least four sensors within a storey, the trigger rate is significantly reduced, improving the purity of the sample selected with the pulse shape recognition trigger.

The parallel operation of two separate RunControl programmes for AMADEUS and the main ANTARES neutrino telescope, which was originally not foreseen, has proven to be very successful. No interference between the two programmes has been observed while the two systems can optimise their detection efficiency and respond to potential problems almost independently. At the same time, both systems profit in the same fashion from developments and improvements of the RunControl software and monitoring tools.

The stability of the system response is excellent. This was verified prior to deployment as well as in situ. It was quantified by observing the mean of the ambient noise distribution as a function of time. In situ, the 10 s of continuous data recorded every hour with the minimum bias trigger were used to calculate the mean. The standard deviation of this value for the first year of operation is less than 2×10^{-5} of the full range.

All sensor types described in Section 2.2 are well suited for the investigation of acoustic particle detection methods. A comparison of the characteristics of the different sensor types will be drawn below.

4.2. Ambient noise

Studies of the power spectral density of the ambient noise at the ANTARES site have been performed using the minimum bias trigger data. Fig. 16 shows the noise levels recorded with representative HTI and ECAP hydrophones and with one AM sensor on Line 12 over several time periods with a combined duration of six months. For each sensor, the power spectral density was calculated for the 10 s intervals of continuous data and then for each 1 kHz bin, the median and the 0.27% quantile (corresponding to a 3σ deviation from the median) were derived for the complete set of measurements. For each sensor, one can observe a characteristic frequency above which the 0.27% quantile of the noise level shows a constant difference to the median. The corresponding frequencies are about 35, 30, and 40 kHz for the HTI hydrophones, ECAP hydrophones and AM sensors, respectively. For higher frequencies, the noise is dominated by the
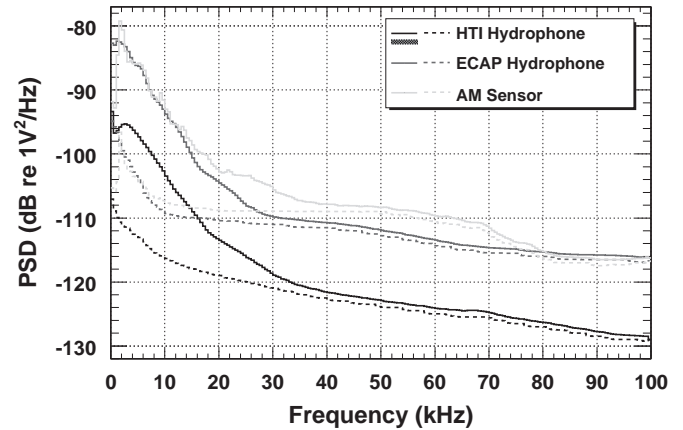

Fig. 16. Power spectral density (PSD) of the noise level recorded in situ. Solid lines represent the median, dotted lines the 0.27% quantile (corresponding to a 3σ deviation from the median). The voltage used is the calibrated input voltage of the AcouADC board.
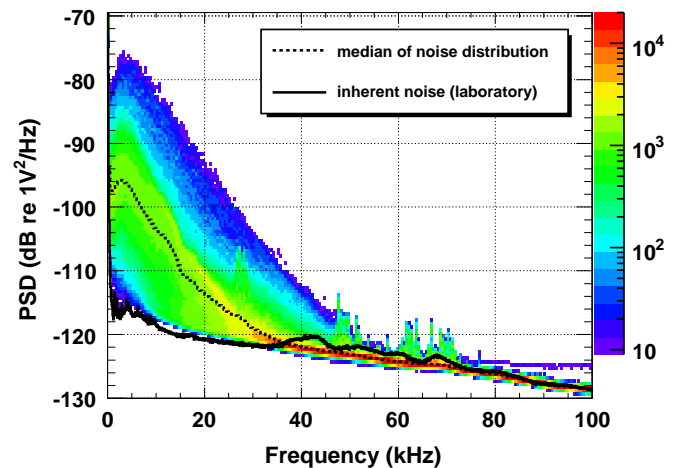

Fig. 17. Power spectral density (PSD) of the ambient noise recorded with one HTI sensor on the topmost storey of the IL. The voltage used is the calibrated input voltage of the AcouADC board. Shown in shades of grey is the occurrence rate in arbitrary units, where dark colours indicate higher rates. Shown as a white dotted line is the median value of the in situ PSD and as a black solid line the noise level recorded in the laboratory prior to deployment.

intrinsic electronics noise, limiting the capability to study the acoustic noise.

The noise floor is the lowest for the HTI hydrophones, the difference in the power spectral density to the ECAP hydrophones and AM sensors being 10–15 dB. When recording transient signals, the effect on the signal-to-noise ratio is partially compensated by the higher sensitivity of the ECAP hydrophones and the AM sensors. The noise spectrum of the AM sensor displays some structure for frequencies up to about 25 kHz. This is due to coupling of the sensor to the glass spheres. In summary, for studies of the in situ ambient noise, the HTI hydrophones are the most suited type of sensors.

In Fig. 17 a more detailed presentation of the noise data recorded with an HTI hydrophone during the year of 2008 is given. An algorithm to remove strong transient signals (mostly coming from the emitters of the acoustic positioning system) was applied. The relics of such signals and electronics noise show up as spikes between 45 and 75 kHz. The lowest level of recorded noise in situ was confirmed to be consistent with the inherent noise of the system recorded in the laboratory prior to deployment. The observed in situ noise can be seen to go below the noise

level measured in the laboratory for frequencies exceeding 35 kHz. This is due to electronic noise coupling into the system in the laboratory that is absent in the deep sea.

The overall noise levels (i.e. the RMS of the signal amplitudes in each 10 s sample) recorded at the same time with any two active sensors of the same type are correlated at a level above 90%. This shows that the recorded data are indeed representative of the ambient conditions and not determined by the inherent noise of the system.

4.3. Transient signals and dynamic range

The signals recorded with the three different types of acoustic sensors on Line 12 for a common source is shown in Fig. 18. The signals were recorded in May 2010 and were received under an angle of about 65° with respect to the direction pointing vertically upwards. The agreement between the signal shapes can be seen to be very good. For the second positive peak at about 0.20–0.25 s, the AM sensor shows a differing behaviour from the hydrophones, which can be attributed to the coupling of the sensor to the glass sphere.

Bipolar signals selected with the pulse shape recognition trigger typically have a signal-to-noise ratio exceeding 2 for a single sensor. Assuming a noise level of 10 mPa in the frequency range from 1 to 50 kHz, which is a typical level recorded at calm sea, i.e. sea state 0, a signal of 20 mPa can be detected. Such a signal is expected to be emitted from a 2 EeV cascade emerging from a neutrino interaction at a distance of about 200 m [3]. Improving the trigger techniques may further enhance the energy sensitivity. Furthermore, the optimal frequency range must be determined to maximise the signal-to-noise ratio for pulses stemming from neutrino interactions. To conclude on the feasibility of a large-scale acoustic neutrino detector in the deep sea—the main objective pursued with the AMADEUS system—further detailed studies are required.

The maximal pressure amplitude that can be recorded for a gain factor of 10 without saturating the input range of the ADC is about 5 Pa. Usually, only anthropogenic signals originating close to the detector reach this pressure level at the positions of the hydrophones.

The direction and position reconstruction of acoustic point sources are currently being pursued as one of the major
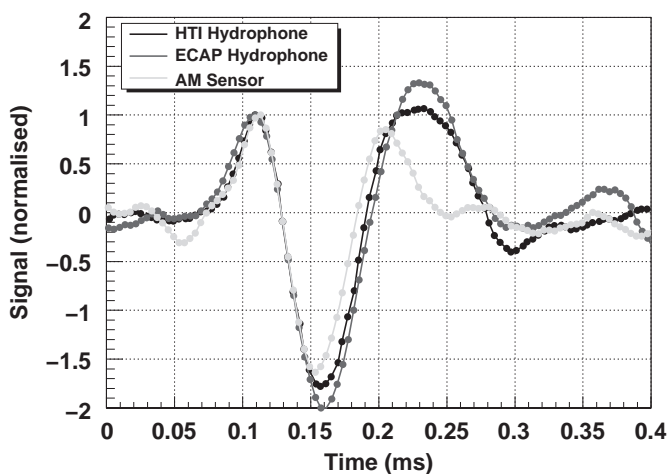

Fig. 19. Typical signals of the ANTARES acoustic positioning system as recorded with four sensors of the AMADEUS system for gain factor 1 of the AcouADC board. For better clarity an offset, starting with 0 V and incremented by 0.5 V with respect to the previous one, is added to the amplitude of each sensor. The first two signals along the time axis were recorded by the acoustic storey holding AMs (see Fig. 1). The following two signals were recorded with two hydrophones on the acoustic storey just above—one hydrophone mounted at the bottom and the other one at the top of the storey. The time is counted since the start of the run.

prerequisites to identify neutrino-like signals. First results are presented in Refs. [15,28].

4.4. Position calibration of acoustic storeys

Just as for the PMTs in the standard storeys, the relative positions of the acoustic sensors within the detector have to be continuously monitored. This is done by using the emitter signals of the ANTARES acoustic positioning system (see Section 2.1). Fig. 19 shows such a signal as recorded by four typical sensors. The delays between the signal arrival times are clearly visible: short delays of less than 1 ms within each storey and a long delay of about 10 ms between the signals arriving in two different storeys.

The time shown in the figure is given in seconds since the start of the run and can be converted into UTC using the data recorded by the clock system (see Section 3.6). As the emission times of the positioning signals are also recorded in UTC, the time difference between emission and reception of the signal can be calculated. Using the signals from multiple emitters and their known positions at the anchors of the lines, the positions of the AMADEUS sensors can be reconstructed.

The position calibration has statistical uncertainties of a few millimetres for each hydrophone. Systematic uncertainties due to the size of the receiving piezo-elements, the knowledge of their relative positions within the acoustic storey, the knowledge of the speed of sound in sea water and the position uncertainties of the emitters are still under study. For the AMs, the position reconstruction is less precise and has a statistical uncertainty of the order of a centimetre.

5. Summary and conclusions

The AMADEUS system for the investigation of techniques for acoustic particle detection in the deep sea has been integrated into the ANTARES neutrino telescope in the Mediterranean Sea at water depths between 2050 and 2300 m. The system started to take data in December 2007 and was completed in May 2008. It

Fig. 18. Comparison of the signals originating from a common source as recorded by three different types of acoustic sensors, each one located on a different storey of Line 12. For better comparability, the first peak of each signal has been normalised to 1 and the time axis of each signal adjusted such that the times of the zero crossings between the first positive and negative peak coincide.
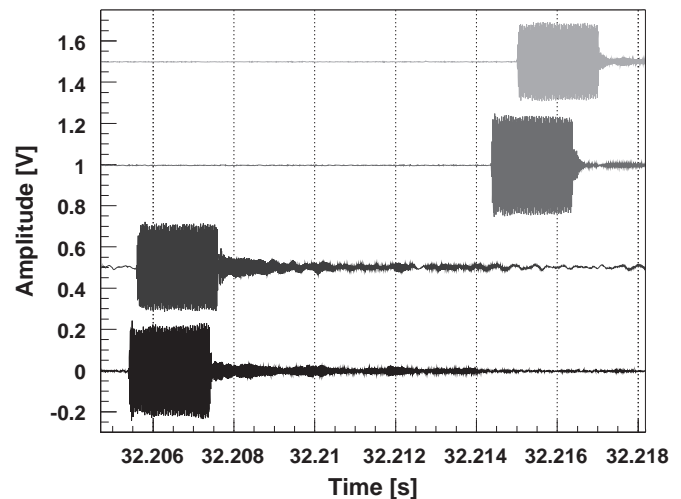
comprises 36 acoustic sensors, of which currently 34 are operational, arranged in six acoustic clusters. Different configurations of sensor clusters are used. The sensors consist of piezoelectric elements and two-stage preamplifiers with combined sensitivities around -145 dB re 1 V/μ Pa.

For the off-shore data acquisition, a dedicated electronics board has been designed. One of 12 steps of analogue amplification between 1 and 562 can be set with the on-shore control software. Data sampling is done at 500 kSps with 16 bits and an analogue anti-alias filter with a 3 dB point at a frequency of 128 kHz. Digital downsampling with factors of 2 and 4 is implemented inside an off-shore FPGA. This value is also selectable using on-shore control software. The system parameters were tuned using the data collected with the autonomous precursor device AMADEUS-0 that was deployed and subsequently recovered at the ANTARES site in March 2005.

Where appropriate, the components of the AMADEUS system have been calibrated in the laboratory prior to deployment; the in situ performance is in full accordance with the expectations. Data taking is going on continuously and the data are recorded if one of three adjustable trigger conditions is met.

The system is well suited to conclude on the feasibility of a future large-scale acoustic neutrino telescope in the deep sea. Furthermore, it has the potential of a multi-purpose device, combining its design goal to investigate acoustic neutrino detection techniques with the potential to perform marine science studies. AMADEUS is a promising starting point for instrumenting the future neutrino telescope project KM3NeT [29,30] with acoustic sensors for position calibration and science purposes.

Acknowledgments

References

[1] G.A. Askariyan, B.A. Dolgoshein, et al., Nucl. Instr. and Meth. 164 (1979) 267.
[2] J. Learned, Phys. Rev. D 19 (1979) 3293.
[3] S. Bevan, et al., ACoRNE Collaboration, Astropart. Phys. 28 (3) (2007) 366 arXiv:astro-ph/0704.1025v1.
[4] S. Bevan, et al., ACoRNE Collaboration, Nucl. Instr. and Meth. A 607 (2009) 389 arXiv:0903.0949v2 [astro-ph.IM].
[5] V. Niess, V. Bertin, Astropart. Phys. 26 (2006) 243 arXiv:astro-ph/0511617v3.
[6] F. Descamps for the IceCube Collaboration, in: Proceedings of the 31st International Cosmic Ray Conference, 2009, arXiv:0908.3251v2 [astro-ph.IM].
[7] K. Antipin, et al., BAIKAL Collaboration, in: Proceedings of the 30th International Cosmic Ray Conference, 2007, arXiv:0710.3113 [astro-ph].
[8] J. Vandenbroucke, G. Gratta, N. Lehtinen, Astrophys. J. 621 (2005) 301 arXiv:astro-ph/0406105.
[9] S. Danaher for the ACoRNE Collaboration, in: Proceedings of ARENA 2006, the Second International Workshop on Acoustic and Radio EeV Neutrino Detection Activities, J. Phys. Conf. Ser. 81, IOP Publishing, Philadelphia, 2007, p. 012011.
[10] G. Riccobene for the NEMO Collaboration, Nucl. Instr. Meth. A 604 (2009) 149.
[11] The ANTARES Collaboration, ANTARES, the first operational Neutrino Telescope in the Mediterranean Sea, Nucl. Instr. and Meth. A, submitted for publication.
[12] M. Ageron, et al., ANTARES Collaboration, Astropart. Phys. 31 (2009) 277 arXiv: 0812.2095 v1 [astro-ph].
[13] P. Amram, et al., ANTARES Collaboration, Nucl. Instr. and Meth. A 484 (2002) 369.
[14] M. Ardid for the ANTARES Collaboration, Nucl. Instr. Meth. A 602 (2009) 174.
[15] C. Richardt, et al., Astropart. Phys. 31 (2009) 19 arXiv:0906.1718v1 [astro-ph.IM].
[16] M. Ageron, et al., ANTARES Collaboration, Nucl. Instr. and Meth. A 581 (2007) 695.
[17] F. Deffner, Studie zur akustischen Neutrinodetektion: Analyse und Filterung akustischer Daten aus der Tiefsee, Diploma Thesis, Univ. Erlangen-Nürnberg, FAU-PI1-DIPL-07-001, 2007, Obtainable from: ⟨http://www.antares.physik. uni-erlangen.de/publications⟩.
[18] G. Anton, et al., Astropart. Phys. 26 (2006) 301.
[19] K. Graf, Experimental studies within ANTARES towards acoustic detection of ultra-high energy neutrinos in the deep sea, Ph.D. Thesis, Univ. Erlangen-Nürnberg, FAU-PI1-DISS-08-001, 2008, Obtainable from: ⟨http://www. antares.physik.uni-erlangen.de/publications⟩.
[20] R.J. Urick, Ambient Noise in the Sea, Peninsula Publishing, Los Altos, USA, 1986, ISBN 0-932146-13-9.
[21] C.L. Naumann, Development of sensors for the acoustic detection of ultra high energy neutrinos in the deep sea, Ph.D. Thesis, Univ. Erlangen-Nürnberg, FAU-PI4-DISS-07-002, 2007, Obtainable from: ⟨http://www.antares.physik. uni-erlangen.de/publications⟩.
[22] J.A. Aguilar, et al., ANTARES Collaboration, Nucl. Instr. and Meth. A 570 (2007) 107.
[23] J.A. Aguilar, et al., ANTARES Collaboration, Nucl. Instr. and Meth. A 622 (2010) 59 arXiv:1007.2549v1 [astro-ph.IM].
[24] R.J. Urick, Principles of Underwater Sound, Peninsula Publishing, Los Altos, USA, 1983, ISBN 0-932146-62-7.
[25] J.A. Aguilar, et al., ANTARES Collaboration, Astropart. Phys. 26 (2006) 314.
[26] F. Rademakers, R. Brun, Root: an object-oriented data analysis framework, Linux Journal 51 ⟨http://root.cern.ch/⟩.
[27] M. Neff, Studie zur akustischen Teilchendetektion im Rahmen des ANTARES-Experiments: Entwicklung und Integration von Datennahmesoftware, Diploma Thesis, Univ. Erlangen-Nürnberg, FAU-PI1-DIPL-07-003, 2007, Obtainable from: ⟨http://www.antares.physik.uni-erlangen.de/publications⟩.
[28] C. Richardt, et al., Nucl. Instr. Meth. A 604 (2009) 189.
[29] U.F. Katz, et al., KM3NeT Consortium, Nucl. Instr. Meth. A 602 (2009) 40.
[30] KM3NeT Consortium, Conceptual Design for a Deep-Sea Research Infrastructure Incorporating a Very Large Volume Neutrino Telescope in the Mediterranean Sea, ISBN 978-90-6488-031-5 ⟨http://www.km3net.org/CDR/ CDR-KM3NeT.pdf⟩, 2008.